Selected for a Viewpoint in *Physics*

PHYSICAL REVIEW B **80**, 014114 (2009)

Atomic-resolution three-dimensional imaging of germanium self-interstitials near a surface: Aberration-corrected transmission electron microscopy

D. Alloyeau,[1,*,†] B. Freitag,[2] S. Dag,[3] Lin W. Wang,[3] and C. Kisielowski[1,*,‡]

[1]*National Center for Electron Microscopy, Lawrence Berkeley National Laboratory, Berkeley, California 94720, USA*

[2]*FEI Company, Eindhoven, Building AAE, Achtseweg Noord 5, P.O. Box 80066, 5600 KA Eindhoven, The Netherlands*

[3]*Scientific Computing Group, Computational Research Division, Lawrence Berkeley National Laboratory, Berkeley, California 94720, USA*

(Received 10 April 2009; revised manuscript received 27 May 2009; published 27 July 2009)

We report the formation and direct observation of self-interstitials in surface proximity of an elemental semiconductor by exploiting subthreshold effects in a new generation of aberration-corrected transmission electron microscopes. We find that the germanium interstitial atoms reside close to hexagonal, tetragonal, and *S*-interstitial sites. Using phase-contrast microscopy, we demonstrate that the three-dimensional position of interstitial atoms can be determined from contrast analysis, with subnanometer precision along the electron-beam direction. Comparison with a first-principles study suggests a strong influence of the surface proximity or a positively charged interstitial. More generally, our investigation demonstrates that imaging of single atom can now be utilized to directly visualize single-defect formation and migration. These high-resolution electron microscopy studies are applicable to a wide range of materials since the reported noise level of the images even allows the detection of single-light atoms.

DOI: 10.1103/PhysRevB.80.014114 PACS number(s): 61.72.jj, 61.72.uf, 68.37.Og, 31.15.es

I. INTRODUCTION

Point defects in elemental semiconductors are broadly studied because they have a large impact on electrical properties and diffusion phenomena,[1] which are the basis for integrated circuit technology. In experimental studies, the application of spectroscopic methods dominates the field,[2–5] but such techniques do not permit the direct observation of defect structures and diffusion paths. On the theoretical side, the calculations often yield inconsistent results. In germanium (Ge), for example, previous calculations suggest that the ⟨110⟩-split interstitial configuration (*D* site) has the lowest energy for the electrically neutral native interstitial point defect.[6–11] Conversely, the theoretical results concerning the relative stability of the hexagonal (*H*) and the tetragonal (*T*) sites do not agree.[6–10] Here we show that single germanium self-interstitial atoms (Ge_i) and their diffusion paths can be directly recorded in lattice images by employing the new generation of electron microscopes that is developed within DOE's transmission electron aberrations-corrected microscope (TEAM) Project.[12,13] These observations are directly comparable with predictions from density-functional theory (DFT) and open up new ways to study native defects and migration problems in semiconductors.

II. EXPERIMENTAL PROCEDURE

The [110] Ge samples were prepared in cross-section geometry from intrinsic bulk Ge single crystals. Mechanical polishing and ion milling were applied to create electron-transparent regions that are only a few atoms thick at the edge of a hole. The samples prepared were dipped into dilute HF to remove adsorbents and passivate surfaces. This preparation procedure creates a very thin amorphous layer on the sample surface. Due to the high brightness of the electron source of the TEAM column [extreme field emission gun (XFEG)],[14,15] the surface of the germanium sample can be polished using the electron beam itself to thin the specimen in the electron microscope column and further clean surfaces.

The TEAM 0.5 microscope was utilized in transmission mode, employing an acceleration voltage of 300 kV together with a monochromator, an aberration corrector (spherical aberration coefficient=3 μm and fifth-order spherical aberration coefficient=5 mm), and a high-brightness gun.[12] We recorded focus-series images around the Scherzer defocus (step width $\Delta f=1.8$ nm), with an acquisition time of one second and a beam-current density of 4.0×10^4 e/nm^2 after monochromation ($\Delta E\sim0.2$ eV).

Our multislice calculations were carried out with the MAC TEMPAS software package.[16] We simulated a Ge crystal in the [110] zone axis orientation, which included monatomic steps starting from columns with one to seven atoms. The distance between successive atoms in the beam direction is 0.4 nm. Since we analyze regions that are thinner than 2.4 nm (six times 0.4 nm) we disregarded absorption effects[17] but introduced a mechanical vibration factor of 0.04 nm.[12] For comparison with the experiment, the lattice images recorded were normalized by dividing by the mean intensity extracted from reference regions of thin amorphous material or vacuum. By this process, a noise level of 4% was determined from the standard deviation of the intensity in this reference region. Here, we analyze the percentage of maximum contrast (PMC) of the images corresponding to $1-I_n$ for each pixel, where I_n is the normalized intensity.

Theoretical study of Ge_i structure was performed by using the first-principles pseudopotential plane-wave method[18] within the generalized gradient approximation (GGA).[19] Computational calculations presented in this paper have been obtained using the Vienna *ab initio* simulation package (VASP).[20–23] Projector-augmented wave (PAW) pseudopotentials were used for Ge and H atoms,[24] and energy cutoff for

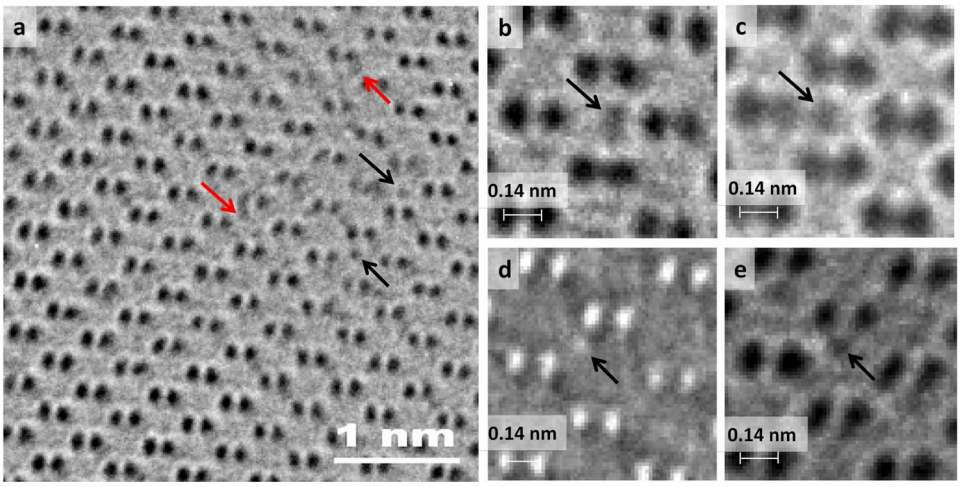

FIG. 1. (Color online) (a) Aberration-corrected images of a thin Ge crystal oriented along the [110] direction [black arrows show occupied interstitial sites, red arrows (dark gray) show column vibrations occurring during the acquisition time]. Magnified areas where an interstitial atom is observed, (b) and (c) In T sites, (d) In an H site that overlaps with a bond-centered site when the crystal is oriented along the [110] zone axis, (e) In an off-center site. Electron dose: 4.0×10^4 electrons/nm^2. Range of focus from −1 to −8 nm.

plane waves was taken as 300 eV. Uniform grids of k points were obtained using the Monkhorst-Pack scheme:[25] $4\times4\times4$, $4\times4\times2$, and $2\times2\times2$ k-point meshes for 64, 128, and 512 atomic sites, respectively. All atomic positions, as well as lattice parameters, have been optimized through lowering total energy, atomic force, and stress. The calculated Ge bulk lattice parameter based on GGA calculations is found as 0.565 nm, which is comparable with the published experimental values.[26]

III. RESULTS

A. Aberration-corrected electron microscopy analysis

In this TEM investigation, Ge self-interstitial atoms were introduced into Ge single crystals by electron irradiation. We recorded phase-contrast images in the [110] projection of wedge-shaped samples. Figure 1(a) is an example that shows the Ge lattice in the [110] projection, as well as localized disturbances, where interstitial atoms are identified. Across the area shown, the sample is only a few atomic layers thick. In the past, only atom columns and extended defects such as stacking faults and dislocations[27–30] could be observed by high-resolution electron microscopy (HREM). Direct imaging of single-defect atoms was not possible because of noise and resolution limitations. Due to the outstanding performance of the TEAM 0.5 microscope, the space between the lattice columns appears mostly empty. As a result, even the 0.14 nm dumbbell distances in germanium [110] can be resolved well beyond the Rayleigh resolution criterion due to the microscope's information transfer of below 0.05 nm.[12] Such performance enables a wealth of direct observations including the imaging of interstitial atoms, the excitation of column oscillations, and the recording of faint traces marking the diffusion paths of interstitial atoms. The interstitial atoms appear at various locations in the projected Ge [110] unit cell as additional contrasts in the void between the lattice columns [Figs. 1(b)–1(e)]. However, these contrasts appear and disappear from frame to frame when image series are recorded with a time of interval of one second. This direct observation of single-atom diffusion in Ge in which migration barriers of less than 1 eV were reported,[31] suggests that the electron beam assists interstitial migration.

In this paper, we focus on extracting the occupied interstitial sites in three dimensions from focal-series experiments, utilizing prior knowledge of the crystal structure. Other aspects of the experiment will be reported elsewhere. The threshold-displacement energy of bulk atoms can be calculated to be 350 keV,[32,33] which exceeds the primary electron-beam energy of 300 keV used in the prototype TEAM 0.5 electron microscope. The atomic column and single-atom positions were determined by fitting Gaussians with subpixel accuracy to the two-dimensional intensity distributions[34] in the images. The mean distance measured between the column positions and the projected hexagonal center of a unit cell exhibits a dispersion (σ) that depends on sample thickness (Fig. 2). In the thicker area of the crystal, a mean-square displacement (σ^2) of 73 pm^2 was determined that increased noticeably to 208 pm^2 in the thinner areas of the sample, where the Ge$_i$ generation is exclusively observed. Therefore, we argue that lattice vibration induced by continuous irradiation is greater in the thinner sample region due to bonds weakening near the surface. Such crystal-lattice excitation and weakened bonds lower the energy threshold for Ge$_i$ formation. Similarly, preferential atom removal from surfaces under electron-beam irradiation due to lowered binding energies was recently reported by Martin *et al.*[35] for the case of gold atoms at the gold-vacuum interface. All these data indicate that the surface effect plays a key role in the formation and the location of Ge$_i$'s, as will be confirmed by our theoretical calculations.

We determined the position of 24 Ge$_i$'s within the projected unit cells of Ge [110]. These single-atom positions are given with respect to the projected hexagonal center of a unit cell [Fig. 3(a)]. A first observation is that the ⟨110⟩-split configuration (D) was never observed. This suggests that this

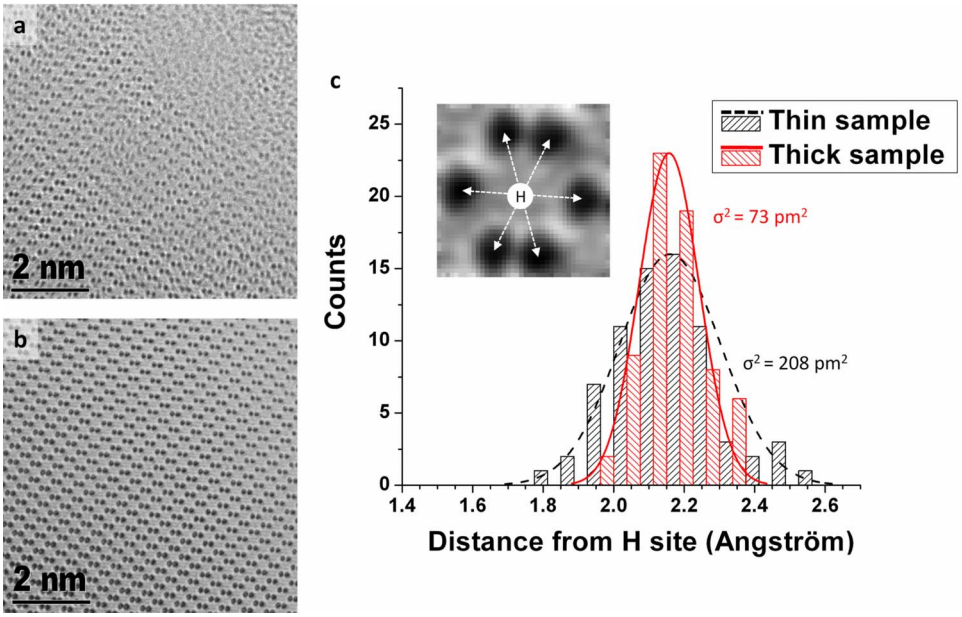

FIG. 2. (Color online) Cs-corrected HRTEM images of a Ge crystal oriented along the [110] direction. (a) Thin area near the sample edge, where excitation of column oscillations and Ge_i formation are observed. (b) Thicker area where we do not observe any disturbances of the crystal lattice. (c) Histograms of the measured distance between the projected atomic columns and the projected hexagonal position in the center of a unit cell (as indicated in the insert). The Gaussian fits show the wider distribution of the measurement in the thin area, highlighting the higher excitation of the column oscillation.

configuration is energetically unstable in a thin Ge crystal, continuously irradiated with 300 keV electrons. Instead, most Ge_i's are localized close to projected *T* [Figs. 1(b) and 1(c)] and *H* sites. Consequently, these are the energetically favored sites in our experiment. However, it is also seen from Fig. 3(a) that the Ge_i's are displaced by 10–40 pm from the geometric *T* or *H* positions. Such large displacements exceed the experimental error for the position determination. The observed deviations from ideal geometric positions are, therefore, physically significant. In extreme cases, we observed Ge_i's shifted in the [−110] direction by 70 pm from the *H* position to an off-center position [Fig. 1(e)]. We also located Ge_i's close to the highly unstable bond-centered site [Fig. 1(d)]. However, the bond-centered sites coincide with other hexagonal sites in the [110] projection.

Through focal series analyses allow access to three-dimensional (3D) and chemical information for TEM samples.[12,36] To begin, we verified that the contrast of the interstitials originates from single Ge atoms by exploiting the dependence of contrast on defocus, as outlined in Ref. 12, for the case of single gold atoms. Image simulations predict the contrast intensity as a function of focal distance as shown in [Fig. 4(a)]. The contrast value at a given focal distance can be used to determine the number of atoms in the projected column and the nature of interstitial atoms. This analysis can best be achieved in a focus window from −6 to −8 nm [Fig. 4(a)], in which the contrast value is flat against the focal distance and the contrast differences between atomic columns of different heights are the greatest. The performance of our analysis is related to the uncommonly small noise

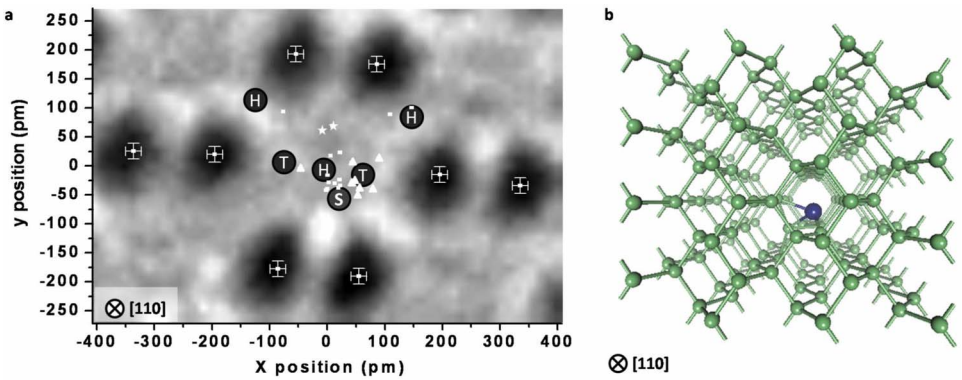

FIG. 3. (Color online) (a) Positions of Ge_i's extracted with subpixel precision from TEM images. The origin of the axis is the central geometrical hexagonal site defined by the surrounding atom columns. Squares with error bar: mean position of the atomic column; Squares: Ge_i's close to the *H* sites; Triangles: Ge_i's close to the *T* sites; Stars: Ge_i's in an off-center position. (b) Model of the new *S* configuration calculated by DFT in a passivated (110) slab of thickness 1.4 nm.

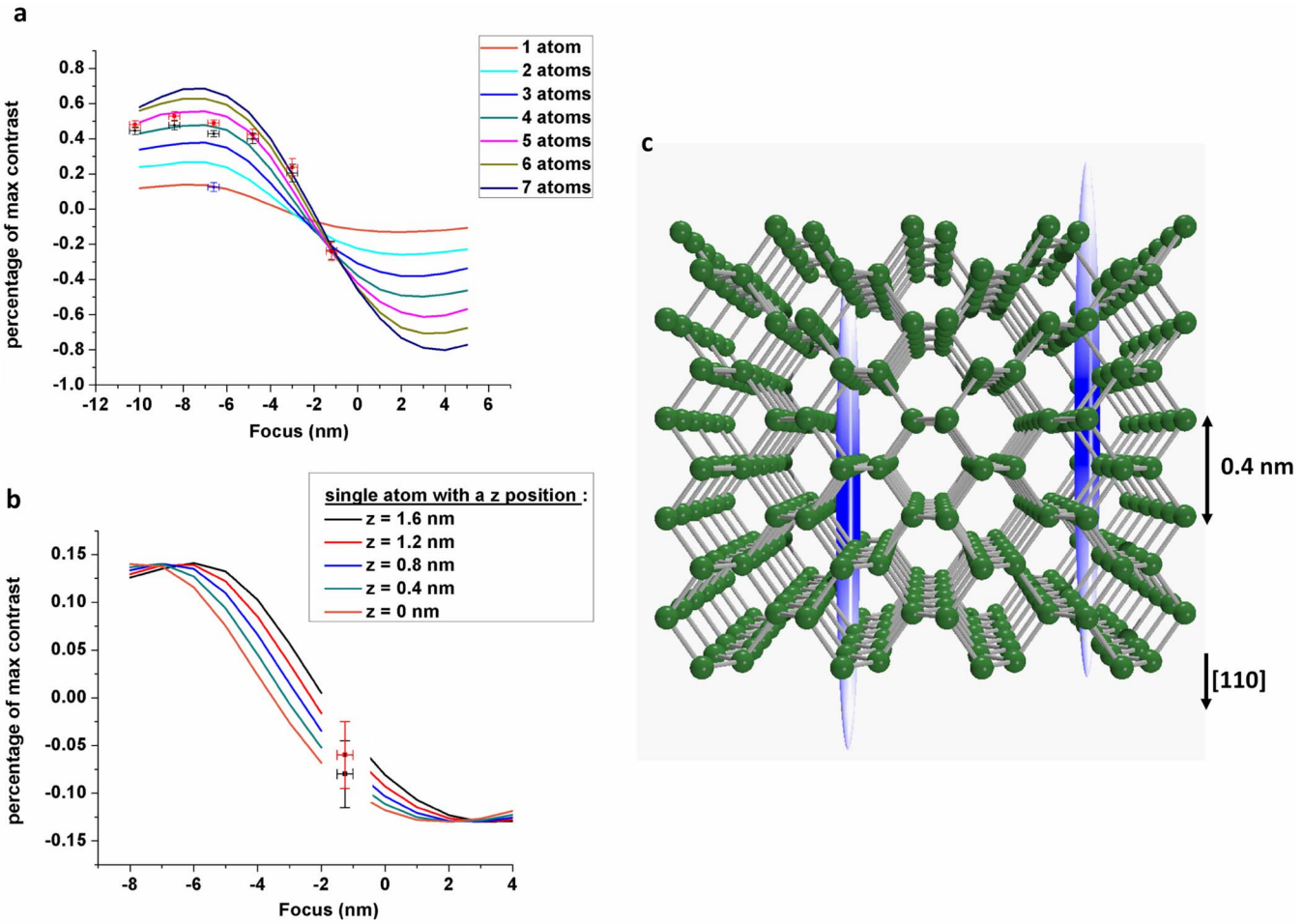

FIG. 4. (Color online) (a) Simulated PMC of Ge atom columns of different heights as a function of focus (curves). The red (dark gray) and black squares present the mean PMC of the atomic columns surrounding the interstitials 1 and 2, respectively, extracted from the experiment. The blue square is the mean PMC of the Ge_i's observed in the micrograph acquired using a focus of −6.6 nm. (b) Contrast of the interstitials 1 and 2 [red (dark gray) and black squares, respectively] compared to the simulated contrast of an interstitial atom located at different z positions. Error bars are given by noise levels: ±4%. (c) 3D representation of the Ge_i's z position in a five-atom high crystal along the [110] direction. The blue cigar shapes represent the position of the interstitials 1 (right cigar) and 2 (left cigar). The elongation of the cigars represents the noise-limited precision of the measurement (±0.9 nm) and scales shaded in blue (gray) gives the probability for the presence of the interstitial along the cigar.

level (±4%) and the high precision of the focus measurement.[12] We measured the percentage of maximum contrast of the interstitials observed in the focus window from −6 to −8 nm, to be 12 ± 2%, which is in perfect agreement with the attenuation of the incoming electron beam calculated for a single Ge atom in a lattice column. This result is also consistent with previous measurements of beam attenuations by single gold (25%)[12] and single carbon (4%)[37] atoms, after an atomic number (Z) dependence of the phase contrast ($I \sim Z^{2/3}$) is taken into account.[17]

In order to determine the depth position of single interstitial atoms (i.e., z position: the position of Ge_i's in the beam direction), we exploit the small focal spread (0.7 nm) of the monochromated TEAM 0.5 electron beam that yields detectable contrast changes even if atomic displacements are only in the order of interatomic distances.[12] Quantitative contrast measurements of Ge_i's were carried out and compared with the contrast of the neighboring atomic columns. In Fig. 4(b), the PMC of Ge interstitials is calculated for different z positions as a function of focus. We have analyzed two interstitial atoms with local focus values of the atomic columns of −1.25 ± 0.25 nm. These interstitials are chosen because in this focus range, contrast changes are most sensitive to displacements in beam direction. The two interstitial atoms chosen were recorded close to the H site [interstitial 1, observed in Fig. 1(d)] and the T site (interstitial 2). By comparing the experiments with simulations [Fig. 4(a)], we found that the atomic columns surrounding these two Ge_i's are either four or five atoms tall. Therefore, for these crystal thicknesses (between 1.2 and 1.6 nm) and focus value (−1.25 nm), the recorded interstitial contrast requires that the two Ge_i atoms reside in the crystal [Fig. 4(b)]. However, the noise-limited precision of the measurement (±0.9 nm) also allows these two Ge_i atoms to be close to the surface [Fig. 4(c)].

B. Density-functional theory study

First-principles calculations were carried out to explain our experimental results and to clarify the discrepancies

TABLE I. Calculated relative energies (eV) of neutral, positively or negatively charged Ge_i's in the *H*, *T*, and *D* configurations. Calculations were performed using both supercells (with 64, 128, and 512 atoms) and hydrogen-passivated clusters. The case labeled "slab" corresponds to a neutral Ge_i in a 1.4-nm-thick passivated crystal. The letters indicate the final structure upon relaxation of an unstable configuration.

System	*H* site	*T* site	*D* site
Ge_i, supercell (64 atoms)	$H \rightarrow T$	0.20	0.0
Ge_i, supercell (128 atoms)	$H \rightarrow T$	0.0	0.16
Ge_i, supercell (512 atoms)	$H \rightarrow T$	0.0	0.30
Ge_i, cluster	0.31	0.56	0.0
Ge_i^-, cluster	0.35	0.51	0.0
Ge_i^+, cluster	0.15	0.0	0.25
Ge_i, slab	$H \rightarrow S$	$T \rightarrow S$	0.11

found in the literature concerning Ge_i structures and locations. The calculations were performed using supercells containing 64, 128, and 512 atoms and a hydrogen-passivated isolated cluster ($Ge_{512}H_{360}$). Calculated self-interstitial energies are listed in Table I.

Our supercell calculations show the importance of the calculation convergence since *D* is the most stable site in the small supercell (64 atoms), whereas *T* becomes energetically favorable for more converged calculations (larger supercells containing 128 and 512 atoms). However, these bulk calculations always indicate that the *H* site is unstable and thus tend to disagree with our TEM investigation where Ge_i positions close to the *H* site are commonly observed. However, when a passivated cluster model is used, the *H* configuration becomes stable, highlighting the quantum-confinement (finite-size) effect on the interstitial energy. More importantly, when a passivated (110) slab with 1.4 nm thickness is used, *H* and *T* sites relax toward a new minimum-energy *S* position, which is energetically more favorable than the *D* site by 0.11 eV. This new configuration shifts away from the geometric *H* and *T* positions by 80 and 90 pm, respectively, and is closer to most of the observed Ge_i positions [Figs. 3(a) and 3(b)]. We have also calculated the effect of charging on the interstitial energy. Only if the Ge_i is positively charged, the *D* site is less stable than the cage-site configurations (*H* or *T* site). Thus, the experimentally observed cage-site configurations can also be explained by a positively charged interstitial, which is not completely unlikely since Ge_i's have a donor level located only 0.04 eV below the conduction-band minimum.[3]

IV. DISCUSSION

Overall, we show here that the results of the calculations are extremely sensitive to the system used. This might explain the diversity of the results in the literature, where the convergence of the calculations and the finite-size effects were not always carefully checked. Our calculations do not take into account lattice excitations induced by the continuous bombardment of the sample by highly energetic electrons. Our column position measurements give a good estimate of the mean-square displacements (σ^2) induced by the electron beam. In the thicker part of the sample, we found a value of $\sigma^2 = 73$ pm^2 which agrees with the Debye-Waller factor for Ge at room temperature reasonably well.[38] Using these published x-ray data, we notice that the temperature must be above 500 K to induce a lattice vibration as important as the electron-beam-induced vibrations in the thinner part of the crystal ($\sigma^2 = 208$ pm^2). The lattice excitation measured in the area where Ge_i's are observed is then energetically significant and can explain any remaining discrepancies between experimental and calculated results. The fact that the atomic details of the sample surface differ from area to area might also be involved.

The new Ge_i *S* configuration calculated for a thin crystal layer similar to the experimental sample highlights the importance of the nearby surfaces, which most likely contribute to the observed Ge_i displacement from geometric *H* and *T* sites. In the experiment, the crystal wedge surface is likely to be passivated by amorphous Ge. In our calculations, removal of the dangling bond is represented by the *H* passivation. The quantum-confinement effect in the experiment and in our slab calculation should also be similar. However, a recent report has shown that the position of an energy minimum along the ⟨111⟩ direction between *T* and *H* sites is charge-state dependent, with a configuration displaced 76 pm from the *H* site, when the interstitial has a single positive charge.[39] Thus, a positive charge state could also be involved in the observed interstitial displacements. Unfortunately, it remains challenging to distinguish between neutral and charged interstitial states by electron microscopy.

Finally, we note that Oh *et al.*[40] recently reported the detection of foreign interstitial gold atoms ($Z=79$) in silicon ($Z=14$), using aberration-corrected scanning transmission electron microscopy. Similarly, unexpected positions of the interstitials were observed. In addition, on closer inspection of these micrographs, slight displacements of the interstitial from the geometrical *T* position are also seen, but remain unaddressed.

V. CONCLUSIONS

We exploited the new performance level of the next generation of electron microscopes to generate and directly observe self-interstitial atoms in the elemental semiconductor Ge. We find that the Ge_i's are generated by subthreshold effects and reside close to hexagonal, tetragonal, and *S*-interstitial sites. Using phase-contrast microscopy, we demonstrate that the 3D position of Ge_i's can be recovered from contrast analysis with subnanometer precision along the electron-beam direction. First-principles calculations suggest a strong influence of the surface proximity or a positive charge state. More generally, our investigation demonstrates that imaging of single atoms can now be utilized to directly visualize single-defect formation and migration. These HREM studies are applicable to a wide range of materials since the reported noise level even allows for the detection of single-light atoms.

ACKNOWLEDGMENTS

We thank Frances Allen for her kind assistance in writing this manuscript. The authors acknowledge support from the National Center for Electron Microscopy, Lawrence Berkeley National Laboratory, which is supported by the (U.S.) Department of Energy, under Contract No. DE-AC02-05CH11231. The TEAM project was supported by the (U.S.) Department of Energy, Office of Science, and Basic Energy Sciences. The detailed image analysis was supported by the Electron Microscopy of Soft Matter Program at Lawrence Berkeley National Laboratory and supported by the Director, Office of Science, Office of Basic Energy Sciences, Materials Sciences and Engineering Division of the (U.S.) Department of Energy under Contract No. DE-AC02-05CH11231. The theoretical part of this work was supported by the DMSE/BES/SC of the (U.S.) Department of Energy under Contract No. DE-AC02-05CH11231. It uses the resources of the National Energy Research Scientific Computing Center.

*Corresponding author.
†FAX: (510) 486-5888; alloyeau.damien@gmail.com
‡cfkisielowski@lbl.gov

[1] H. Mehrer, *Diffusion in Solids*, Springer Series in Solid State Science (Springer, Berlin, 2007).
[2] M. Budde, B. Bech Nielsen, P. Leary, J. Goss, R. Jones, P. R. Briddon, S. Öberg, and S. J. Breuer, Phys. Rev. B **57**, 4397 (1998).
[3] H. Haesslein, R. Sielemann, and C. Zistl, Phys. Rev. Lett. **80**, 2626 (1998).
[4] R. Sielemann, H. Haesslein, and C. Zistl, Physica B **302-303**, 101 (2001).
[5] R. Sielemann, H. Haesslein, L. Wende, and C. Zistl, Physica B **273-274**, 565 (1999).
[6] A. Carvalho, R. Jones, C. Janke, J. P. Goss, P. R. Briddon, J. Coutinho, and S. Oberg, Phys. Rev. Lett. **99**, 175502 (2007).
[7] A. J. R. da Silva, A. Janotti, A. Fazzio, R. J. Baierle, and R. Mota, Phys. Rev. B **62**, 9903 (2000).
[8] G. S. Khoo and C. K. Ong, J. Phys. Chem. Solids **51**, 1177 (1990).
[9] M. D. Moreira, R. H. Miwa, and P. Venezuela, Phys. Rev. B **70**, 115215 (2004).
[10] K. Sueoka and J. Vanhellemont, Mater. Sci. Semicond. Process. **9**, 494 (2006).
[11] J. Vanhellemont, P. Spiewak, and S. Koji, J. Appl. Phys. **101**, 036103 (2007).
[12] C. Kisielowski, B. Freitag, M. Bischoff, H. van Lin, S. Lazar, G. Knippels, P. Tiemeijer, M. van der Stam, S. von Harrach, M. Stekelenburg, M. Haider, S. Uhlemann, H. Miller, P. Hartel, B. Kabius, D. Miller, I. Petrov, E. A. Olson, T. Donchev, E. A. Kenik, A. R. Lupini, J. Bentley, S. J. Pennycook, I. M. Anderson, A. M. Minor, A. K. Schmid, T. Duden, V. Radmilovic, Q. M. Ramasse, M. Watanabe, R. Erni, E. A. Stach, P. Denes, and U. Dahmen, Microsc. Microanal. **14**, 469 (2008).
[13] R. Erni, M. D. Rossell, C. Kisielowski, and U. Dahmen, Phys. Rev. Lett. **102**, 096101 (2009).
[14] B. Freitag, G. Knippels, S. Kujawa, P. C. Tiemeijer, M. Van der Stam, D. Hubert, C. Kisielowski, P. Denes, A. Minor, and U. Dahmen, Microsc. Microanal. **14**, 1370 (2008).
[15] http://www.fei.com/products/types/x-feg.aspx
[16] http://www.totalresolution.com
[17] J. R. Jinschek, C. Kisielowski, D. Van Dyck, and P. Geuens, Proc. SPIE **5187**, 54 (2003).
[18] M. C. Payne, M. P. Teter, D. C. Allan, T. A. Arias, and J. D. Joannopoulos, Rev. Mod. Phys. **64**, 1045 (1992).
[19] J. P. Perdew, J. A. Chevary, S. H. Vosko, K. A. Jackson, M. R. Pederson, D. J. Singh, and C. Fiolhais, Phys. Rev. B **46**, 6671 (1992).
[20] G. Kresse and J. Furthmüller, Comput. Mater. Sci. **6**, 15 (1996).
[21] G. Kresse and J. Furthmüller, Phys. Rev. B **54**, 11169 (1996).
[22] G. Kresse and J. Hafner, Phys. Rev. B **47**, 558 (1993).
[23] G. Kresse and D. Joubert, Phys. Rev. B **59**, 1758 (1999).
[24] P. E. Blöchl, Phys. Rev. B **50**, 17953 (1994).
[25] H. J. Monkhorst and J. D. Pack, Phys. Rev. B **13**, 5188 (1976).
[26] P. Villars and L. D. Calvert, *Pearson's Handbook of Crystallographic Data for Intermetallic Phases* (ASM International, Materials Park, OH, 1991).
[27] J. Desseaux-Thibault, A. Bourret, and J. M. Penisson, Microscopy of Semiconducting Materials, 1983: Proceedings of the Institute of Physics Conference (ISBN: 9780854981588), **67**, 71 (1983).
[28] M. Hirabayashi, K. Hiraga, and D. Shindo, Ultramicroscopy **9**, 197 (1982).
[29] S. Takeda, Jpn. J. Appl. Phys., Part 2 **30**, L639 (1991).
[30] S. Takeda, M. Hirata, S. Muto, G.-C. Hua, K. Hiraga, and M. Kiritani, Ultramicroscopy **39**, 180 (1991).
[31] P. Spiewak, M. Muzyk, K. J. Kurzydlowski, J. Vanhellemont, K. Mlynarczyk, P. Wabinski, and I. Romandic, J. Cryst. Growth **303**, 12 (2007).
[32] J. J. Loferski and P. Rappaport, Phys. Rev. **111**, 432 (1958).
[33] I. M. Robertson and I. Jencic, J. Nucl. Mater. **239**, 273 (1996).
[34] C. Kisielowski, O. Schmidt, and J. Yang, Mater. Res. Soc. Symp. Proc. **482**, 369 (1998).
[35] A. V. Martin, K. Ishizuka, C. Kisielowski, and L. J. Allen, Phys. Rev. B **74**, 172102 (2006).
[36] D. Alloyeau, C. Ricolleau, T. Oikawa, C. Langlois, Y. Le Bouar, and A. Loiseau, Ultramicroscopy **109**, 788 (2009).
[37] J. C. Meyer, C. Kisielowski, R. Erni, M. D. Rossell, M. F. Crommie, and A. Zettl, Nano Lett. **8**, 3582 (2008).
[38] G. Dalba and P. Fornasini, J. Synchrotron Radiat. **4**, 243 (1997).
[39] A. Carvalho, R. Jones, J. P. Goss, C. Janke, and P. R. B. S. Öberg, J. Phys.: Condens. Matter **20**, 135220 (2008).
[40] S. H. Oh, K. Van Benthem, S. I. Molina, A. Y. Borisevich, W. Luo, P. Werner, N. D. Zakharov, D. Kumar, S. T. Pantelides, and S. J. Pennycook, Nano Lett. **8**, 1016 (2008).